Kerr rotation in Cu, Ag, and Au driven by spin accumulation and spin-orbit coupling

Gyung-Min Choi* and David G. Cahill

Department of Materials Science and Engineering and Materials Research Laboratory, University of Illinois, Urbana, Illinois 61801, USA

(Received 11 June 2014; revised manuscript received 20 November 2014; published 19 December 2014)

We measure transient spin accumulation in Cu, Ag, and Au by time-resolved magneto-optical Kerr effect. The transient spin current is generated by ultrafast demagnetization of a ferromagnetic [Co/Pt] layer, and spin accumulates in an adjacent normal metal, Cu, Ag, or Au by spin diffusion. The magnitude of the Kerr rotation is described by an off-diagonal conductivity tensor that is proportional to spin accumulation and spin-orbit coupling. From comparisons between observed Kerr rotations and calculated spin accumulations, we determine the strength of spin-orbit coupling of conduction electrons in Cu, Ag, and Au to be 0.02, 0.01, and 0.12 eV, respectively.

DOI: 10.1103/PhysRevB.90.214432 PACS number(s): 72.25.Ba, 71.70.Ej, 78.20.Ls

I. INTRODUCTION

In metallic spintronic devices, spin injection from a ferromagnet (FM) to a nonmagnetic metal (NM) is a central issue. Experimental investigations of the spin injection require a method to generate spin current from FM and detect spin accumulation in NM. The generation of spin currents has been achieved by passing charge currents through FM [1,2], by passing heat currents through FM [3], by spin pumping [4], and by spin Hall effect [5]. These methods operate on time scales that are long compared to the time scales of spin relaxation and spin diffusion; therefore, the spin currents generated by these methods are essentially in steady state.

Spin accumulation in NM can be detected electrically using a second FM [1,2] or via the inverse spin Hall effect [6]. Recently, optical detection of spin accumulation in NM has been reported [7,8]. Fohr *et al.* used Brillouin light scattering to measure stationary spin accumulation in NM produced by spin pumping [7]. Melnikov *et al.* used the polarization of optical second harmonic generation to measure transient spin accumulation in Au and interpreted the results in terms of spin-dependent transport of hot carriers [8]. In Ref. [8] the constant of proportionality that relates the rotation of polarization and spin accumulation was not studied by either experiment or theory.

Previously we have shown ultrafast demagnetization produces transient spin accumulation in Cu, and spin accumulation can be detected by the linear magneto-optical Kerr effect (MOKE) [9]. Here we extend our work to Ag and Au and develop a model that predicts the magnitude of the Kerr rotation in terms of the strength of spin-orbit coupling. MOKE is conventionally applied to studies of metallic FM and semiconductors. Our results show that spin accumulation in NM also produces a useful MOKE signal that has its origin in spin-orbit coupling.

II. EXPERIMENTAL DETAILS

We prepared FM/NM structure of sapphire substrate/Pt(20)/FM(6)/NM(h) (unit in nm). The FM is a [Co/Pt] multilayer with perpendicular magnetization $\{[\mathrm{Co}(0.4)/\mathrm{Pt}(1)]_{\times 4}/\mathrm{Co}(0.4)\}$, and the NM layer is Cu, Ag, or Au. Depending on thickness of NM, we refer to these samples as the Cu-h, Ag-h, or Au-h sample. Metal layers are deposited by magnetron sputter at the University of Illinois (UIUC). For Cu and Ag samples, we deposit a thin topcoat of SiO_2 by e-beam evaporation to protect Cu and Ag from oxidation or corrosion by sulfides.

The magnetic properties of the [Co/Pt] layer were characterized with a vibrating sample magnetometer by our colleagues at Korea Institute of Science and Technology (KIST): the saturation magnetization is $4 \times 10^5\ \mathrm{A\,m^{-1}}$, the coercivity is 0.09 T, and the remanence is close to one. Electrical conductivities of the Pt, [Co/Pt], Cu, Ag, and Au layers are measured using a four-point probe with separately prepared samples {sapphire/Pt(100),sapphire/Pt(2)/[Co(0.4)/Pt(1)]$_{\times 15}$/Pt(1), sapphire/Cu(100), sapphire/Ag(100), and sapphire/Au(100)} and are summarized in Table I.

We use time-resolved polar MOKE to detect the transient spin accumulation in the direction normal to the film. The light wavelength is 785 nm, and the full-width-at-half-maximum of the pump and probe are $\approx$0.8 and $\approx$ 0.3 ps, respectively. The incident pump fluence is $10.6\ \mathrm{J\,m^{-2}}$; the absorbed fluence is $3.7\ \mathrm{J\,m^{-2}}$. A perpendicular magnetic field of ± 0.3 T was applied to samples before MOKE measurement to set the [Co/Pt] magnetization to $\pm z$ direction. All measurements are done at room temperature without magnetic field.

III. RESULTS AND DISCUSSION

We use ultrafast demagnetization of [Co/Pt] as the source of spin currents [9]. When both pump and probe beams are incident on the Pt side of the samples, we observe a rapid demagnetization of [Co/Pt] on a subpicosecond time scale followed by a slow recovery. By comparing the transient Kerr rotation (ΔM) and static Kerr rotation (M), we determine the peak $\Delta M/M$: 0.25 ± 0.04, 0.25 ± 0.04, and 0.28 ± 0.04, for Cu, Ag, and Au samples, respectively. Therefore, to within experimental uncertainties, the peak change in magnetization is independent of the composition of the NM layer. (The rate of recovery of magnetization is reduced in the Au sample because Au has weaker electron-phonon coupling than Cu or Ag.) The demagnetization data are also independent of the NM thickness. Previously we showed that rapid demagnetization generates spin currents by electron-magnon coupling within [Co/Pt]; the spin generation rate is the negative of the demagnetization rate $-dM/dt$ [9]. The $-dM/dt$ is nearly the same for Cu, Ag, and Au samples [Fig. 1(b)].

*Corresponding author: gchoi11@illinois.edu

TABLE I. Parameters for the spin diffusion calculation in Fig. 3: σ is the in-plane electrical conductivity, N_F is the electronic density of states at the Fermi level, D is the diffusion constant, and τ_S is the spin relaxation time.

	Pt	[Co/Pt]	Cu	Ag	Au
σ ($10^7\,\Omega^{-1}\mathrm{m}^{-1}$)	0.6[a]	0.2[a]	3.9[a]	3.8[a]	2.7[a]
N_F ($10^{47}\,\mathrm{J}^{-1}\mathrm{m}^{-3}$)	11.48[b]	11.16[b]	1.55[b]	0.99[b]	1.08[b]
D ($10^{-3}\,\mathrm{m}^2\mathrm{s}^{-1}$)	0.21	0.074	9.8	15	9.8
τ_S (ps)	0.3	0.01	16	1.5	0.4

[a]Obtained from four-point probe measurement.
[b]Obtained from the electronic heat capacity of Ref. [11].

Spin generated in [Co/Pt] accumulates in NM via spin diffusion [9]. In Fig. 2 we plot time-resolved measurements of the spin accumulation in NM by probing Kerr rotation at the surface of NM; the probe beam is incident on the Cu, Ag, or Au side of the samples while the pump beam is incident on the Pt side of the samples. The Kerr rotation changes sign when the [Co/Pt] magnetization is changed from the $+z$ to the $-z$ direction and closely resembles the rate of change of magnetization plotted in Fig. 1(b). At a NM thickness of 100 nm, the peak Kerr rotation is the highest in Au, but it decreases more quickly with thickness than Cu and Ag. {While the Kerr rotation directly generated by demagnetization of [Co/Pt] is negligible on the NM side of the Cu-100 and Ag-100 samples, it has a small contribution to the Kerr rotation in the Au-100 sample. We subtracted the expected demagnetization signal from the Kerr rotation of the Au-100 sample to get the true spin accumulation signal (see Appendix A).}

Following our previous work [9], we quantify the spin accumulation by solving the spin diffusion equation [10]

$$\frac{\partial \mu_S}{\partial t} = D\frac{\partial^2 \mu_S}{\partial z^2} - \frac{\mu_S}{\tau_S}, \tag{1}$$

where $\mu_S = \mu_\uparrow - \mu_\downarrow$ is the spin chemical potential, D is the spin diffusion constant, and τ_S is the spin relaxation time. The D of Pt, [Co/Pt], Cu, and Au are calculated by $D = \frac{\sigma}{e^2 N_F}$, where σ is the electrical conductivity and N_F is the density of states at the Fermi level, $N_F = \frac{3\gamma}{\pi^2 k_B^2}$, where γ is the electronic heat capacity coefficient [11] and k_B is the Boltzmann constant. The τ_S is related to the spin diffusion length l_S, $\tau_S = \frac{l_S^2}{D}$. The

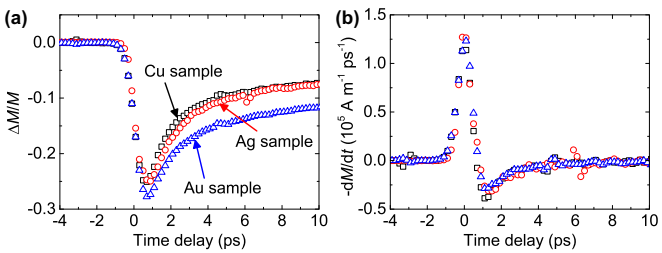

FIG. 1. (Color online) (a) Demagnetization data measured on the Pt side of the Cu-100 (black squares), Ag-100 (red circles), and Au-100 (blue triangles) samples. (b) The $-dM/dt$ of the Cu-100 (black squares), Ag-100 (red circles), and Au-100 (blue triangles) samples. Data are obtained by multiplying the saturation magnetization $4 \times 10^5\,\mathrm{A\,m^{-1}}$ by numerical differention of (a).

l_S values at room temperature are reported to be 7–10 nm for Pt [12,13], 350–500 nm for Cu [2,14], 150 nm for Ag [15], and 60 nm for Au [14]. Assuming l_S of 8, 400, 150, and 60 nm, we obtain τ_S of 0.3, 16, 1.5, and 0.4 ps for Pt, Cu, Ag, and Au, respectively.

The τ_S of the FM is a critical parameter in the modeling. In our prior work we studied the spin transfer torque in a Pt (30)/[Co/Pt/Co/Ni] (6.4)/Cu (10)/CoFeB (2) sample grown at KIST [9]. A spin diffusion simulation with $\tau_S = 0.05$ ps for [Co/Pt/Co/Ni], estimated from the theory of Elliot-Yafet, was in good agreement with the measured spin transfer torque [9] but with some discrepancy. To better constrain τ_S, we re-analyzed the spin transfer torque measurement [9] with τ_S as a free parameter and find $\tau_S = 0.02$ ps of [Co/Pt/Co/Ni] produces the best fit between the measurement and the model (see Appendix B).

Comparison of the Kerr rotation of Cu samples with a FM layer of [Co/Pt/Co/Ni] (grown at KIST) and Cu samples with a FM layer of [Co/Pt] (grown at UIUC) shows that the Kerr rotation is approximately two times larger with the KIST [Co/Pt/Co/Ni] FM layer than the UIUC [Co/Pt] FM layer (see Appendix B). As we discuss in more detail below, spin accumulation in Cu is approximately proportional to τ_S of the FM. Therefore, we determine $\tau_S = 0.01$ ps for the UIUC [Co/Pt] FM layers. We expect this small τ_S of [Co/Pt] is due to multiple interfaces between Co and Pt. Recently, the interface spin-flipping parameter δ at the Co/Pt interface was reported to be $0.9^{+0.5}_{-0.2}$, which leads to the spin-flipping probability of $0.6^{+0.2}_{-0.1}$ at the interface by $P = 1 - \exp(-\delta)$ [16]. Values of D and τ_S of each layer are summarized in Table I.

We solve the coupled diffusion equations for Cu-h, Ag-h, and Au-h samples by equating μ_S at interfaces and setting the spin generation rate of [Co/Pt] to be $-dM/dt$. The predicted spin accumulation n_S, $\mu_S = 2\frac{n_S}{N_F}$, at the surface of NM is shown in Fig. 3. The calculation is in good agreement with the positions of the positive-negative peaks and the thickness dependence. At the same NM thickness, the spin accumulation is the largest in Cu because of its relatively long l_S and large N_F.

The thickness dependence of the Kerr rotation can be explained with l_S of NM. While it has a weak dependence on the thickness in Cu and Ag, spin accumulation shows a much stronger dependence on the Au thickness due to the short l_S (Fig. 4). From the thickness dependence of the peak Kerr rotation in Au, we determine $l_S = 60 \pm 10$ nm, which leads to $\tau_S = 0.4 \pm 0.1$ ps. Melnikov *et al.* observed a spin signal in Fe/Au structures and interpreted their data using a model based on ballistic transport of hot carriers [8]. From this analysis, the authors of Ref. [8] obtained a hot-carrier $\tau_S = 1.2$ ps for Au [8]. Our result of $\tau_S = 0.4$ ps, obtained from diffusive transport, is an important point of comparison with Ref. [8].

The τ_S of each layer has a different effect on spin accumulation in NM. The τ_S of Pt does not affect the spin accumulation in NM because the low diffusivity of [Co/Pt] essentially decouples Pt from NM. The τ_S of [Co/Pt] has a dominant role in the spin accumulation in NM as it is the smallest time scale: spin accumulation in NM is approximately proportional to the τ_S of [Co/Pt]. At the NM thickness of 100 nm, the τ_S of Cu or Ag has little effect on the spin

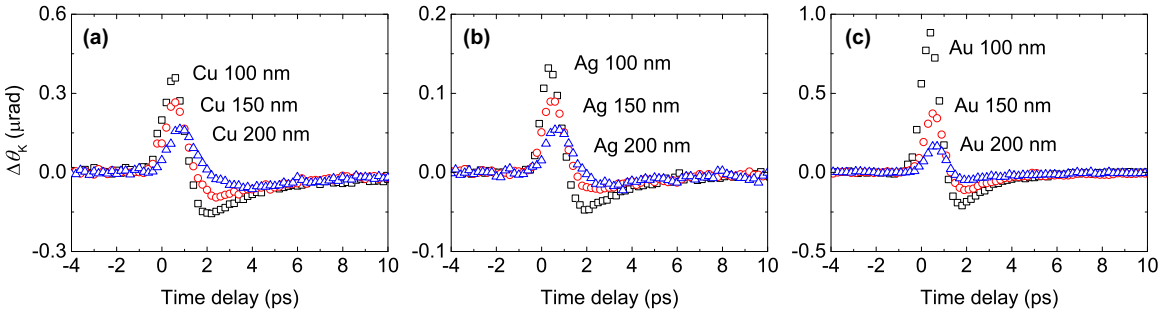

FIG. 2. (Color online) The Kerr rotations measured on the NM side of the (a) Cu-h, (b) Ag-h, and (c) Au-h samples: black squares, red circles, and blue triangles are for NM thickness of 100, 150, and 200 nm, respectively.

accumulation due to relatively long τ_S, while the τ_S of Au has a significant effect (see Appendix B). Therefore, the important parameters are τ_S of [Co/Pt] (grown at UIUC) and Au, which are determined experimentally to be 0.01 and 0.4 ps.

The polar Kerr rotation of cubic metals driven by a magnetic perturbation can be expressed as [17,18]

$$\tilde{\theta}_K = \frac{\varepsilon_{xy}}{(\varepsilon_{xx}-1)\sqrt{\varepsilon_{xx}}} = \frac{\sigma_{xy}}{\sigma_{xx}\sqrt{1+\frac{i}{\omega\varepsilon_0}\sigma_{xx}}}, \quad (2)$$

where ε_{ij} is the complex dielectric tensor and σ_{ij} is the complex conductivity tensor, which are related by $\varepsilon_{ij} = \delta_{ij} + \frac{i}{\omega\varepsilon_0}\sigma_{ij}$, ε_0 is the vacuum permittivity, and ω is the light frequency. The conductivity tensor has contributions from interband and intraband transitions. Because our photon energy ($\hbar\omega =$ 1.58 eV) cannot reach the d bands of Cu, Ag, or Au which lie >2 eV below the Fermi level, we assume that only intraband transitions contribute to the Kerr rotation.

The conventional way to describe intraband transition is the Drude model. Within the assumptions of the Drude model, the diagonal and off-diagonal conductivity tensors are

$$\sigma_{xx} = \omega_P^2\varepsilon_0\frac{(1/\tau - i\omega)}{(1/\tau - i\omega)^2 + \omega_C^2} \approx i\frac{\omega_P^2\varepsilon_0}{\omega}, \quad (3)$$

$$\sigma_{xy} = \omega_P^2\varepsilon_0\frac{\omega_C}{(1/\tau - i\omega)^2 + \omega_C^2} \approx -\left(\frac{\omega_P}{\omega}\right)^2\varepsilon_0\omega_C, \quad (4)$$

where ω_P is the plasma frequency, $\omega_P = \sqrt{\frac{ne^2}{m*\varepsilon_0}}$, n is electron concentration, e is electron charge, m^* is effective mass, and ω_C is the cyclotron frequency, $\omega_C = \frac{eB}{m*}$, and B is the magnetic field. Taking n from the free electron model and m^* from Ref. [19] ($n = 8.45\times10^{28}$, 5.85×10^{28}, and 5.9×10^{28} m^{-3} for Cu, Ag, and Au, respectively, and $m^* = 1.5\,m_e$ for Cu and $m^* = m_e$ for Ag and Au, where m_e is the electron rest mass), $\hbar\omega_P$ is 8.8, 9.0, and 9.0 eV for Cu, Ag, and Au, respectively. The approximation on the right-hand side of the equation is the limit of $\omega \gg 1/\tau$ and $\omega \gg \omega_C$.

Kerr rotation of nonmagnetic metals (Al, Cu, Ag, and Au) has been investigated by applying a static magnetic field [17,18] and explained by ω_C. Although a magnetic field can also produce spin accumulation by splitting the energy of spin subbands, the ω_C term dominates the measured Kerr rotation in noble metals.

Elezzabi *et al.* reported the Kerr rotation of a Au film induced by a transient magnetic field with a picosecond rise time [20]. They interpreted the Kerr rotation as a result of the magnetic field driven spin accumulation and obtained $\tau_S \approx 45$ ps from the time delay between magnetic field and Kerr rotation. We argue, however, that the Kerr rotation observed in Ref. [20] has significant contribution from ω_C. Substituting (3) and (4) into (2), the magnetic field driven Kerr rotation is

$$\tilde{\theta}_K = i\frac{\omega_C}{\omega}\frac{1}{\sqrt{1-\frac{\omega_P^2}{\omega^2}}} \approx \frac{\omega_C}{\omega_P}. \quad (5)$$

The peak magnetic field of 50 mT of Ref. [20] produces $\hbar\omega_C \approx 6\times10^{-6}$ eV. Using $\hbar\omega_P = 9.0$ eV, the Kerr rotation is ≈0.7 μrad, which is comparable to the observation of 0.45 μrad of Ref. [20]. Furthermore, $\tau_S \approx 45$ ps is inconsistent with a l_S of 60 nm of Au.

In materials such as TmS, TmSe, and Gd, it has been reported that the magnetic field driven Kerr rotation can have

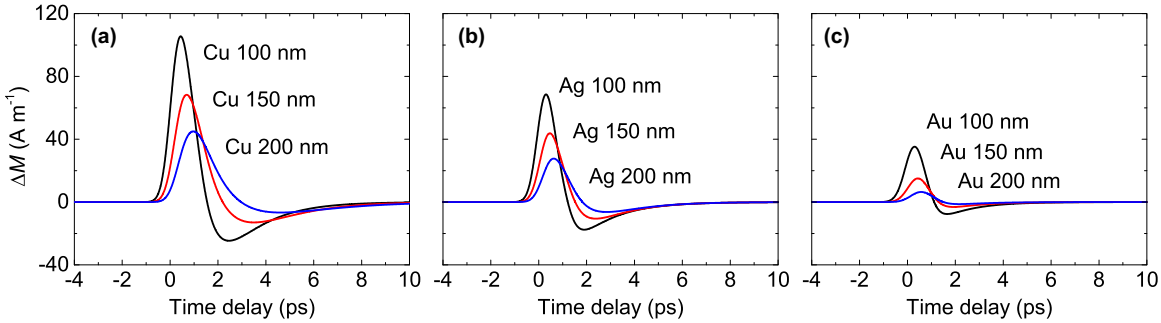

FIG. 3. (Color online) The calculated spin accumulations at the NM surface of the (a) Cu-h, (b) Ag-h, and (c) Au-h samples: black, red, and blue lines are for NM thickness of 100, 150, and 200 nm, respectively.

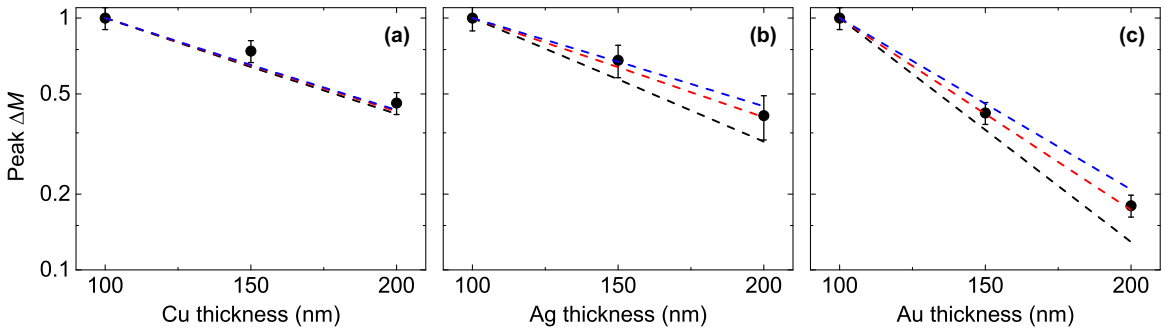

FIG. 4. (Color online) The dependence of the peak spin accumulation on the (a) Cu, (b) Ag, and (c) Au thicknesses. (a) Black circles are experimental data from Fig. 2(a) and solid lines are from calculation [black, red, and blue lines are for l_S of Cu of 300 ($\tau_S = 9$ ps), 400 ($\tau_S = 16$ ps), and 500 ($\tau_S = 26$ ps) nm, respectively]. (b) Black circles are experimental data from Fig. 2(b); solid lines are from calculation [black, red, and blue lines are for l_S of Ag of 100 ($\tau_S = 0.7$ ps), 150 ($\tau_S = 1.5$ ps), and 200 ($\tau_S = 2.7$ ps) nm, respectively]. (c) Black circles are experimental data from Fig. 2(c); solid lines are from calculation [black, red, and blue lines are for l_S of Au of 50 ($\tau_S = 0.3$ ps), 60 ($\tau_S = 0.4$ ps), and 70 ($\tau_S = 0.5$ ps) nm, respectively].

a significant contribution from spin accumulation [21–23]. However, in noble metals, the magnetic field driven Kerr rotation mostly comes from ω_C. Since we produce spin accumulation from demagnetization of a ferromagnet without a magnetic field, spin accumulation should be the only source of Kerr rotation in our experiments. We find no Kerr rotation in a control sample of Pt/Au (without [Co/Pt]), in which there is no demagnetization-induced spin accumulation.

Kerr rotation driven by spin accumulation can be described by skew scattering theory [21–23]. The contribution of spin accumulation to the off-diagonal conductivity tensor is

$$\sigma_{xy} = \frac{n_\uparrow - n_\downarrow}{n_\uparrow + n_\downarrow}\left(\omega_P^2 \varepsilon_0\right)\left[\frac{\Omega}{(1/\tau - i\omega)^2 + \Omega^2} - \frac{P_0}{e v_F} \times\left(1 - \frac{i\omega(1/\tau - i\omega)}{(1/\tau - i\omega)^2 + \Omega^2}\right)\right], \quad (6)$$

where Ω is the skew scattering frequency, P_0 is the maximum macroscopic dipole moment, and v_F is the Fermi velocity. The first term in the square bracket was used to explain the Kerr rotation of TmS and TmSe [22], and the second term was used to explain the Kerr rotation of Gd [21]. When $\omega \gg 1/\tau$ and $\omega \gg \Omega$, the first term in the square bracket gives a mostly real contribution to $\tilde{\theta}_K$; the second term gives a mostly imaginary contribution to $\tilde{\theta}_K$. In our experiments, the imaginary part of $\tilde{\theta}_K$ is a factor of >5 smaller than the real part and we conclude that the first term is dominant over the second term. Substituting (6) into (2), and taking the limit $\omega \gg 1/\tau$ and $\omega \gg \Omega$,

$$\tilde{\theta}_K = i\frac{n_\uparrow - n_\downarrow}{n_\uparrow + n_\downarrow}\left(\frac{\Omega}{\omega}\right)\frac{1}{\sqrt{1 - \frac{\omega_P^2}{\omega^2}}} \approx \frac{n_\uparrow - n_\downarrow}{n_\uparrow + n_\downarrow}\left(\frac{\Omega}{\omega_P}\right). \quad (7)$$

We determine Ω for Cu, Ag, and Au by comparing the measured Kerr rotations (Fig. 2) and calculated spin accumulations (Fig. 3) for the Cu-100, Ag-100, and Au-100 samples. With $n_\uparrow - n_\downarrow$ from the peak spin accumulation in Fig. 3 divided by the Bohr magneton and $n_\uparrow + n_\downarrow$ from the free electron model, $\frac{n_\uparrow - n_\downarrow}{n_\uparrow + n_\downarrow}$ are 1.35×10^{-4}, 1.26×10^{-4}, and 0.64×10^{-4} for Cu-100, Ag-100, and Au-100, respectively. By comparing the experimental Kerr rotation with Eq. (7), we find $\hbar\Omega = 0.02$, 0.01, and 0.12 eV for Cu, Ag, and Au, respectively.

We equate $\hbar\Omega$ with the strength of spin-orbit coupling in the conduction band. The atomic spin-orbit splittings are 0.25 eV for Cu $3d$, 0.03 eV for Cu $4p$, 0.55 eV for Ag $4d$, 0.11 eV for Ag $5p$, 1.52 eV for Au $5d$, and 0.47 eV for Au $6p$ [24], which are much larger than our values of $\hbar\Omega$. We speculate that the small values of $\hbar\Omega$ in our experiments can be attributed to the fact that the conduction band has mostly s character and that the spin-orbit coupling we observe is generated by weak s-d or s-p hybridization. It is surprising that $\hbar\Omega$ of Ag is smaller than Cu despite larger atomic spin-orbit splitting. We speculate that the small $\hbar\Omega$ of Ag is due to the fact that the d band of Ag lies ≈4 eV below the Fermi level, a factor of ≈2 larger than Cu and Au. We also perform identical experiments with a Pt (20)/[Co/Pt] (6)/Al (100) sample and find no Kerr rotation presumably due to extremely small spin-orbit coupling in Al.

We note that an energy splitting of 0.11 eV for the surface states of Au (111) has been reported using photoemission spectra and interpreted as a result of spin-orbit coupling due to s-p hybridization of the surface state [25]. Photoemission spectra were unable to resolve the energy splitting of Cu (111) or Ag (111) surface states [26]; theory predicts orders of magnitude smaller values of the splitting for Cu(111) or Ag(111) than Au (111) [27]. We also discuss other possible mechanisms in Appendix C.

IV. CONCLUSION

In summary, we achieve optical detection of spin accumulation in Cu, Ag, and Au on subpicosecond time scales. The magnitude of spin signal is described by the product of spin accumulation and spin-orbit coupling. Our results provide a direct measurement of spin-orbit coupling of conduction electrons in Cu, Ag, and Au.

ACKNOWLEDGMENTS

This work was supported by the Army Research Office under Grant No. W911NF-14-1-0016. TR-MOKE measurement was carried out in the Laser and Spectroscopy Laboratory of the Materials Research Laboratory at UIUC. We acknowledge

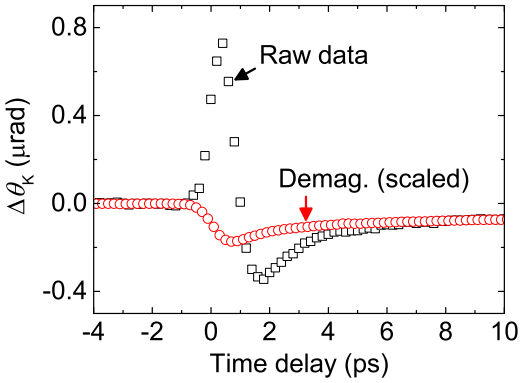

FIG. 5. (Color online) The raw Kerr rotation measured on the Au side of the Au-100 sample (black squares) and the demagnetization signal (red circles), which is scaled to match the Kerr rotation at 10 ps. The $\Delta\theta$ by spin accumulation of the Au-100 sample in Fig. 2(c) is obtained by subtracting the demagnetization signal from the raw Kerr rotation.

C. H. Moon, B. C. Min (KIST), and K. J. Lee (Korea University) for measurements of magnetic properties and discussions.

APPENDIX A: SUBTRACTION OF DEMAGNETIZATION

For TR-MOKE measurements from the NM side of samples, the Kerr rotation generated by directly by the demagnetization of [Co/Pt] decreases exponentially with increasing NM layer thickness,

$$\Delta\theta_{\text{Demag}} \propto \exp\left(-\frac{4\pi\kappa h}{\lambda}\right), \tag{A1}$$

where κ is the extinction coefficient of NM, h is the thickness of NM, and λ is the wavelength of light. At a NM thickness of 100 nm, $\Delta\theta_{\text{Demag}}$ is much smaller than $\Delta\theta$ created by spin accumulation in the Cu-100 and Ag-100 samples, but $\Delta\theta_{\text{Demag}}$ is not negligible in the Au-100 sample due to smaller κ and uncertainty in thickness: From the light transmission and ellipsometry measurements we determine the κ to be 5.6 ± 0.3 and 4.9 ± 0.3 for Cu and Au, respectively; the uncertainty of thickness of NM is $\approx$10%. To extract $\Delta\theta$ due only to spin accumulation from the data, we subtract the residual demagnetization signal from the raw data with a scaling factor set by assuming that the negative offset of the raw data at 10 ps is due to $\Delta\theta_{\text{Demag}}$ (Fig. 5).

APPENDIX B: DETERMINATION OF τ_S Of [Co/Pt]

In our previous work, we presented spin transfer torque (STT) results for a sapphire substrate/Pt(30)/[Co/Pt/Co/Ni] (6.4)/Cu(10)/CoFeB(2)/MgO(10)/Al_2O_3(5) (unit in nm), sample grown at KIST, where [Co/Pt/Co/Ni] represents [Co(0.4)/Pt(1)]$_{x4}$/Co(0.2)/Ni(0.4)/Co(0.2) [9]. Due to spin current generated by demagnetization of the [Co/Pt/Co/Ni] layer, STT tilts the CoFeB magnetization and leads to subsequent precession of the magnetization. In Ref. [9] the amplitude of the CoFeB precession was explained by assuming a value for the spin relaxation time of [Co/Pt/Co/Ni] (τ_S = 0.05 ps) derived from the theory of Elliot-Yafet [28,29].

To obtain more accurate value of τ_S, we use τ_S as a free parameter in the analysis of the STT experiment described in Ref. [9]. The precession amplitude of the CoFeB magnetization is determined by the spin current (J_S) that is absorbed by CoFeB. We calculate J_S by solving spin diffusion equation (1) with a boundary condition of $\mu_S = 0$ in the CoFeB layer. We find from our models that J_S is proportional to τ_S of [Co/Pt].

We also include finite spin conductances at FM/NM interfaces because the interfacial spin conductance becomes dominant over the bulk diffusivity when the thickness of the Cu layer is 10 nm. For the longitudinal component, the spin conductance is $\frac{G_\uparrow+G_\downarrow}{2e^2}$, and for the transverse component the spin conductance is $\frac{\text{Re}\{G_{\uparrow\downarrow}\}}{e^2}$, where $G_{\uparrow,\downarrow}$ is the conductance of the spin up/down and $G_{\uparrow\downarrow}$ is the spin mixing conductance [30]. We use the longitudinal spin conductance at Pt/[Co/Pt/Co/Ni] and [Co/Pt/Co/Ni]/Cu interfaces and the transverse spin conductance at Cu/CoFeB interface. The electrical conductance $G_\uparrow + G_\downarrow$ at the Co/Cu interface has been reported to be $0.75 \times 10^{15}\ \Omega^{-1}\,\text{m}^{-2}$ from theoretical calculation [31] and $2 \times 10^{15}\ \Omega^{-1}\,\text{m}^{-2}$ from experimental measurement [32]. Since the Co layer at Co/Cu interface is very thin, 0.2 nm, we expect the adjacent layer Ni also affects the electrical conductance of at the Co/Cu interface: Experimentally measured electric conductance is $5.6 \times 10^{15}\ \Omega^{-1}\,\text{m}^{-2}$ for the Ni/Cu interface [33]. Considering these values, we use

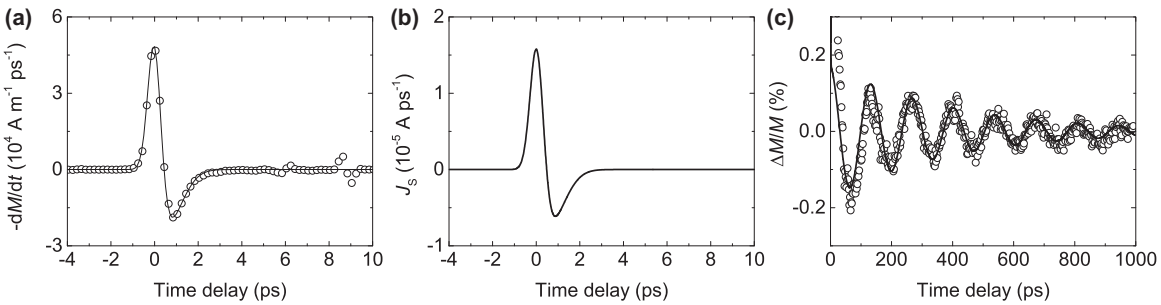

FIG. 6. The STT result with the [Co/Pt/Co/Ni] layer, grown at KIST. (a) The $-dM/dt$ of [Co/Pt/Co/Ni] (black circles), obtained from the demagnetization data of Ref. [9]. Solid line is a fit to a Gaussian function. (b) The calculated spin current that is absorbed by the CoFeB layer in the Pt (30)/[Co/Pt/Co/Ni] (6.4)/Cu (10)/CoFeB (2) (unit in nm) sample with $\tau_S = 0.02$ ps of [Co/Pt/Co/Ni]. (c) The precession data (black circles) and simulation result (solid lines) of the CoFeB precession of the Pt (30)/[Co/Pt/Co/Ni] (6.4)/Cu (10)/CoFeB (2) sample: the data are taken from Ref. [9]; the simulation is based on Eq. (B1) with an input spin current of (b).

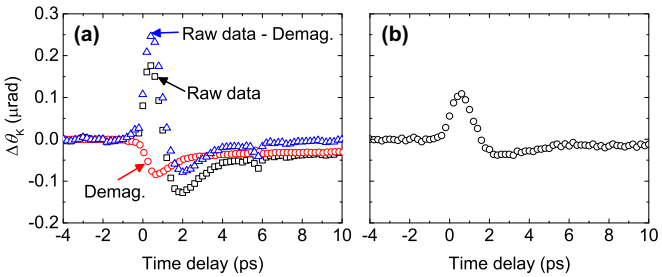

FIG. 7. (Color online) The comparison of the spin accumulation data of [Co/Pt/Co/Ni], grown at KIST, and [Co/Pt], grown at UIUC. (a) The Kerr rotation measured on the Cu side of the Pt (30)/[Co/Pt/Co/Ni] (6.4)/Cu (80) (unit in nm) sample (black squares): The $\Delta\theta$ by spin accumulation (blue triangles) is obtained by subtracting the demagnetization signal (red circles) from the raw Kerr rotation. (b) The Kerr rotation measured on the Cu side of the Pt (30)/[Co/Pt] (6)/Cu (100) (unit in nm) sample (black circles). All data are taken from Ref. [9].

$G_\uparrow + G_\downarrow$ of $3 \times 10^{15}\,\Omega^{-1}\,\mathrm{m}^{-2}$ for the [Co/Pt/Co/Ni]/Cu interface. For the Pt/Co interface, experimentally measured electric conductance is $1.2 \times 10^{15}\,\Omega^{-1}\,\mathrm{m}^{-2}$ [34]. Considering the small thickness of Co adjacent to Pt, we use $1.5 \times 10^{15}\,\Omega^{-1}\,\mathrm{m}^{-2}$ for the Pt/[Co/Pt/Co/Ni] interface. For the Cu/CoFeB interface we use $G_{\uparrow\downarrow}$ of $0.56 \times 10^{15}\,\Omega^{-1}\,\mathrm{m}^{-2}$ from theoretical calculation for the Co/Cu interface [31]. In Fig. 6(b) we calculate J_S with these spin conductances and τ_S of 0.02 ps for [Co/Pt/Co/Ni].

With J_S as an input, we perform magnetization dynamics simulations for CoFeB with the Landau-Lifshitz-Gilbert equation incorporating STT [35],

$$\dot{\mathbf{m}} = -\gamma \mathbf{m} \times \mathbf{H}_{\mathrm{eff}} + \alpha \mathbf{m} \times \dot{\mathbf{m}} + \frac{J_S}{M_S h} \mathbf{m} \times (\mathbf{m} \times \mathbf{m}_{\mathrm{fixed}}), \tag{B1}$$

where $\mathbf{m}$ and $\mathbf{m}_{\mathrm{fixed}}$ are unit vectors in the direction of the CoFeB and [Co/Pt/Co/Ni] magnetizations, $\dot{\mathbf{m}}$ is the time derivative of $\mathbf{m}$, $M_S = 1.2 \times 10^6\,\mathrm{A\,m^{-1}}$ and $h = 2$ nm are the saturation magnetization and thickness of the CoFeB layer, $\mathbf{H}_{\mathrm{eff}}$ is the effective field due to applied field of 0.045 T and shape anisotropy of CoFeB, γ is the gyromagnetic ratio, $\alpha = 0.02$ is the Gilbert damping constant of CoFeB, and J_S is the spin current. The τ_S of [Co/Pt/Co/Ni] determines J_S, and J_S determines the precession amplitude of CoFeB. From the fitting of the measured CoFeB precession with Eq. (B1), we determine τ_S of [Co/Pt/Co/Ni] to be 0.02 ps [Fig. 6(c)].

The fit depends on the choices of spin conductances at FM/NM interfaces. When we reduce $G_\uparrow + G_\downarrow$ of the [Co/Pt/Co/Ni]/Cu interface to $0.75 \times 10^{15}\,\Omega^{-1}\,\mathrm{m}^{-2}$, the value we used in Ref. [9], the best fit is $\tau_S = 0.03$ ps for [Co/Pt/Co/Ni]. (The spin conductance of the Pt/[Co/Pt/Co/Ni] does not affect the fitting because the low diffusivity of [Co/Pt/Co/Ni] nearly decouples spin current that flows into Pt from the spin current that flows into Cu. For the Cu/CoFeB interface we cannot estimate the uncertainty in the spin conductance due to the lack of experimental reports of $G_{\uparrow\downarrow}$ but the single theoretical calculation of Ref. [31].)

In Ref. [9] we showed spin accumulation data for two different structures: sample 1 is the sapphire substrate/Pt(30)/[Co/Pt/Co/Ni] (6.4)/Cu(80)/MgO(10)/Al_2O_3(5) (unit in nm), grown at KIST; sample 2 is the sapphire substrate/Pt(30)/[Co/Pt](6)/Cu(100)/SiO_2(10) (unit in nm), grown at UIUC: [Co/Pt/Co/Ni] represents $[\mathrm{Co}(0.4)/\mathrm{Pt}(1)]_{x4}/\mathrm{Co}(0.2)/\mathrm{Ni}(0.4)/\mathrm{Co}(0.2)$ and [Co/Pt] represents $[\mathrm{Co}(0.4)/\mathrm{Pt}(1)]_{x4}/\mathrm{Co}(0.4)$. For sample 1, $\Delta\theta_{\mathrm{Demag}}$ is not negligible because Cu 80 nm is not thick enough to completely suppress the demagnetization signal. To derive the contribution to $\Delta\theta$ produced by spin accumulation of sample 1, we subtract the residual demagnetization signal from the raw data [Fig. 7(a)]. Given the same $-dM/dt$, the $\Delta\theta$ by spin accumulation of sample 2 is approximately a factor of 2 smaller than that of sample 1 [Fig. 7(b)].

The spin accumulation in Cu at the thickness of ≈100 nm is proportional to τ_S of [Co/Pt], while τ_S of Pt and Cu does not affect the spin accumulation significantly (Fig. 8). From this proportionality and $\tau_S = 0.02$ ps of [Co/Pt/Co/Ni] (grown at KIST), we determine τ_S of [Co/Pt] (grown at UIUC) to be 0.01 ps. Table II summarizes the peak $\Delta\theta$ by spin accumulation and the associated τ_S of different sample structures.

APPENDIX C: OTHER POSSIBLE MECHANISMS

Ultrafast demagnetization generates THz electric fields [36]. We rule out any contribution from THz generation in our measurements for two reasons. First, THz radiation is proportional to the second time derivative of magnetization

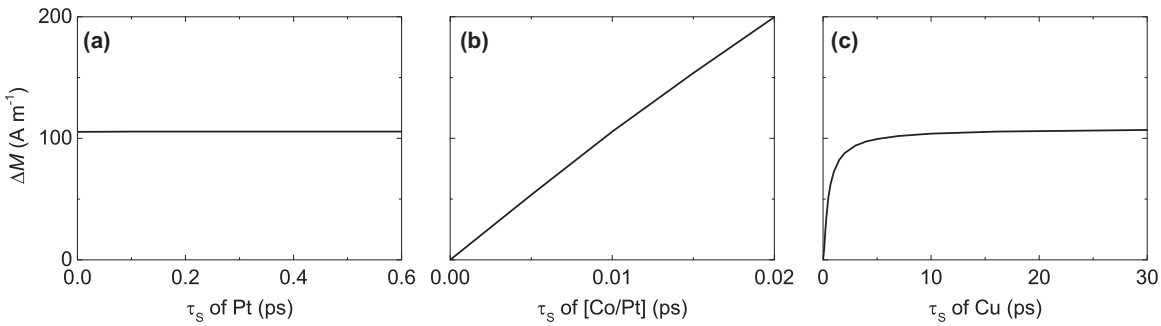

FIG. 8. The dependence of the spin accumulation on the spin relaxation time of Pt, [Co/Pt], and Cu in the Pt (20)/[Co/Pt] (6)/Cu (100) (unit in nm) structure. (a) The τ_S of Pt is varied from 0 to 0.6 ps while τ_S of [Co/Pt] and Cu are fixed at 0.01 and 16 ps, respectively. (b) The τ_S of [Co/Pt] is varied from 0 to 0.02 ps while τ_S of Pt and Cu are fixed at 0.3 and 16 ps, respectively. (c) The τ_S of Cu is varied from 0 to 30 ps while τ_S of Pt and [Co/Pt] are fixed at 0.3 and 0.01 ps, respectively.

TABLE II. Comparison of spin accumulation of different sample structures: $\Delta M/M$ is the peak demagnetization of FM ([Co/Pt/Co/Ni] or [Co/Pt]), $\Delta\theta_K$ is the peak Kerr rotation on Cu, and τ_S is the spin relaxation time of FM. Data of samples 1 and 2 are taken from Ref. [9] and data of sample 3 are taken from Fig. 2(a). Sample 1 is grown at KIST and samples 2 and 3 are grown at UIUC.

	$\Delta M/M$	$\Delta\theta_K$ (μrad)	τ_S(ps)
Sample 1[a]	0.08	0.18 (0.25[b])	0.02
Sample 2[c]	0.08	0.11	0.01
Sample 3[d]	0.25	0.36	0.01

[a]Pt(30)/[Co(0.4)/Pt(1)]$_{\times 4}$/Co(0.2)/Ni(0.4)/Co(0.2)/Cu(80) (unit in nm).
[b]Value after subtracting demagnetization signal from raw data.
[c]Pt(30)/[Co(0.4)/Pt(1)]$_{\times 4}$/Co(0.4)/Cu(100) (unit in nm).
[d]Pt(20)/[Co(0.4)/Pt(1)]$_{\times 4}$/Co(0.4)/Cu(100) (unit in nm).

while our result of the Kerr rotation is explained by the first time derivative of magnetization (Figs. 2 and 3). Second, THz radiation should not produce the time delays and broadenings of the signal that we observe in our data within increasing thickness of NM layers.

Ultrafast demagnetization can also produce eddy currents in metallic ferromagnetic layers. We rule out any contribution from eddy currents in our measurements for two reasons. First, if eddy currents are a dominant mechanism for the Kerr rotation measured on Cu, Ag, and Au, the Kerr rotation should be nearly the same for Cu, Ag, and Au because the electrical conductivities are similar for our Cu, Ag, and Au samples. The measured Kerr rotations of Ag and Au differ by nearly one order of magnitude (Fig. 2). Second, the dependence of the Kerr rotation on the thickness of Cu, Ag, and Au is well explained by spin relaxation lengths of Cu, Ag, and Au that are consistent with reported values (Fig. 4).

[1] M. Johnson and R. H. Silsbee, Phys. Rev. Lett. **55**, 1790 (1985).
[2] F. J. Jedema, A. T. Filip, and B. J. van Wees, Nature (London) **410**, 345 (2001).
[3] A. Slachter, F. L. Bakker, J-P. Adam, and B. J. van Wees, Nat. Phys. **6**, 879 (2010).
[4] Y. Tserkovnyak, A. Brataas, and G. E. W. Bauer, Phys. Rev. Lett. **88**, 117601 (2002).
[5] S. O. Valenzuela and M. Tinkham, Nature (London) **442**, 176 (2006).
[6] T. Kimura, Y. Otani, T. Sato, S. Takahashi, and S. Maekawa, Phys. Rev. Lett. **98**, 156601 (2007).
[7] F. Fohr, S. Kaltenborn, J. Hamrle, H. Schultheiss, A. A. Serga, H. C. Schneider, B. Hillebrands, Y. Fukuma, L. Wang, and Y. Otani, Phys. Rev. Lett. **106**, 226601 (2011).
[8] A. Melnikov, I. Razdolski, T. O. Wehling, E. T. Papaioannou, V. Roddatis, P. Fumagalli, O. Aktsipetrov, A. I. Lichtenstein, and U. Bovensiepen, Phys. Rev. Lett. **107**, 076601 (2011).
[9] G.-M. Choi, B.-C. Min, K.-J. Lee, and D. G. Cahill, Nat. Commun. **5**, 4334 (2014).
[10] T. Valet and A. Fert, Phys. Rev. B **48**, 7099 (1993).
[11] A. Tari, *The Specific Heat of Matter at Low Temperatures* (Imperial College Press, London, 2003).
[12] L. Vila, T. Kimura, and Y. C. Otani, Phys. Rev. Lett. **99**, 226604 (2007).
[13] Y. Niimi, D. Wei, H. Idzuchi, T. Wakamura, T. Kato, and Y. C. Otani, Phys. Rev. Lett. **110**, 016805 (2013).
[14] T. Kimura, J. Hamrle, and Y. Otani, Phys. Rev. B **72**, 014461 (2005).
[15] R. Godfrey and M. Johnson, Phys. Rev. Lett. **96**, 136601 (2006).
[16] H. Y. T. Nguyen, W. P. Pratt, Jr., and J. Bass, J. Magn. Magn. Mater. **361**, 30 (2014).
[17] E. A. Stern, J. C. McGroddy, and W. E. Harte, Phys. Rev. **135**, A1306 (1964).
[18] S. E. Schnatterly, Phys. Rev. **183**, 664 (1969).
[19] P. B. Johnson and R. W. Christy, Phys. Rev. B **6**, 4370 (1972).
[20] A. Y. Elezzabi, M. R. Freeman, and M. Johnson, Phys. Rev. Lett. **77**, 3220 (1996).
[21] J. L. Erskine and E. A. Stern, Phys. Rev. B **8**, 1239 (1973).
[22] W. Reim *et al.*, J. Appl. Phys. **55**, 2155 (1984).
[23] W. Reim and J. Schoenes, *Ferromagnetic Materials*, edited by K. H. J. Buschow and E. P. Wohlfarth (Elsevier, New York, 1990), Chap. 2.
[24] C. E. Moore, *Atomic Energy Levels* (National Bureau of Standards, Washington, DC, 1949).
[25] S. LaShell, B. A. McDougall, and E. Jensen, Phys. Rev. Lett. **77**, 3419 (1996).
[26] G. Nicolay, F. Reinert, S. Hüfner, and P. Blaha, Phys. Rev. B **65**, 033407 (2001).
[27] G. Bihlmayer, Yu. M. Koroteev, P. M. Echenique, E. V. Chulkov, and S. Blűgel, Surf. Sci. **600**, 3888 (2006).
[28] R. J. Elliot, Phys. Rev. **96**, 266 (1954).
[29] Y. Yafet, *Solid State Physics*, edited by F. Seitz and D. Turnbull (Academic, New York, 1963), Vol. 14.
[30] J. Barnaś, A. Fert, M. Gmitra, I. Weymann, and V. K. Dugaev, Phys. Rev. B **72**, 024426 (2005).
[31] M. Zwierzycki, Y. Tserkovnyak, P. J. Kelly, A. Brataas, and G. E. W. Bauer, Phys. Rev. B **71**, 064420 (2005).
[32] J. Bass and W. P. Pratt, Jr., J. Magn. Magn. Mater. **200**, 274 (1999).
[33] C. E. Moreau, I. C. Moraru, N. O. Birge, and W. P. Pratt, Jr., Appl. Phys. Lett. **90**, 012101 (2007).
[34] A. Sharma *et al.*, J. Appl. Phys. **102**, 113916 (2007).
[35] J. C. Slonczewski, J. Magn. Magn. Mater. **247**, 324 (2002).
[36] E. Beaurepaire *et al.*, Appl. Phys. Lett. **84**, 3465 (2004).